IEEE Access
Multidisciplinary | Rapid Review | Open Access Journal

Received 19 May 2023, accepted 30 May 2023, date of publication 7 June 2023, date of current version 14 June 2023.

Digital Object Identifier 10.1109/ACCESS.2023.3283908

SURVEY

Design Considerations of Capacitive Power Transfer Systems

HUSSEIN MAHDI[1], (Graduate Student Member, IEEE), REIJI HATTORI[2], (Member, IEEE), BJARTE HOFF[1], (Senior Member, IEEE), ANYU UEZU[2], AND KATSUMI AKIYOSHI[2]

[1]Department of Electrical Engineering, UiT The Arctic University of Norway, 8514 Narvik, Norway
[2]Interdisciplinary Graduate School of Engineering Sciences, Kyushu University, Fukuoka 816-8580, Japan

Corresponding author: Hussein Mahdi (hussein.al-sallami@uit.no)

This work was supported by the Grant from the Publication Fund of UiT The Arctic University of Norway.

ABSTRACT Capacitive power transfer (CPT) is a near-field wireless power transfer (WPT) technology that has attracted attention in different charging applications. By utilizing electric fields, CPT gives charging systems advantages in terms of cost, weight, flexibility, and mobility. This paper surveys a number of empirical published works in a period between 2015 and 2023. Additionally, it discusses theoretical and practical design considerations of a CPT system to understand and improve the technology and its applications. The paper studies the one- and two-port measuring approaches using vector network analyzers to determine the coupling parameters and compares the measurements to the simulated values using COMSOL Multiphysics©. The two-port approach gives more accurate results than the one-port approach. The paper designs and tests a 13.56 MHz CPT system using the two-port measurement results. The system transfers 100 W at 87.4% efficiency and 30 mm separation distance. Lastly, the paper discusses the design limitations and challenges of the CPT systems, aiming to emphasize the design obstacles that can drive the advancement of the CPT systems for wireless charging applications.

INDEX TERMS Wireless power transmission, capacitive power transfer, couplings, VNA, two-port.

I. INTRODUCTION

Wireless power transfer (WPT) has received considerable attention in various electric charging applications. The International Telecommunication Union [1] defines WPT as "*the transmission of power from a power source to an electrical load using the electromagnetic field.*" Near-field WPT, or "non-beam" WPT, is a non-radiative propagation WPT technique in which the sizes of the transmitter and the receiver are much smaller than the wavelength of the electromagnetic waves [2]. It can transfer low to medium levels of electric power over a range of hundreds of millimeters without mechanical contact and using simple to moderate system architecture. It provides an autonomous, safe, flexible, and reliable charging approach for high-power charging applications.

The associate editor coordinating the review of this manuscript and approving it for publication was Alon Kuperman.

Near-field WPT is categorized into magnetic field coupling and electric field coupling based on the type of coupling. Magnetic coupling, or Inductive Power Transfer (IPT), transfers power between a power source and an electrical load by means of magnetic fields. Capacitive coupling, or Capacitive Power Transfer (CPT), wirelessly transfers power using alternating electric fields confined between conductors. IPT systems typically employ basic compensation circuits with systems' efficiency greater than 90% [3]. Besides, they can transfer higher power levels across larger separation distances compared to CPT systems [4]. Unlike magnetic field coupling based WPT technologies, CPT has some merits, including lightweight, low-cost, low eddy-losses in nearby metals, and good misalignment tolerance [3], [4], [5], [6].

Capacitive charging provides solutions in many applications such as safety fields, consumer electronics, transport, electric machines, biomedical, and miscellaneous applications [7]. For transport charging applications, CPT was proposed to charge on-road vehicles [8],

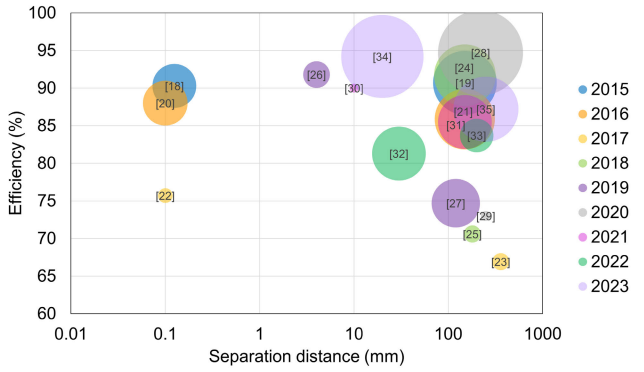

FIGURE 1. System efficiency versus separation distance.

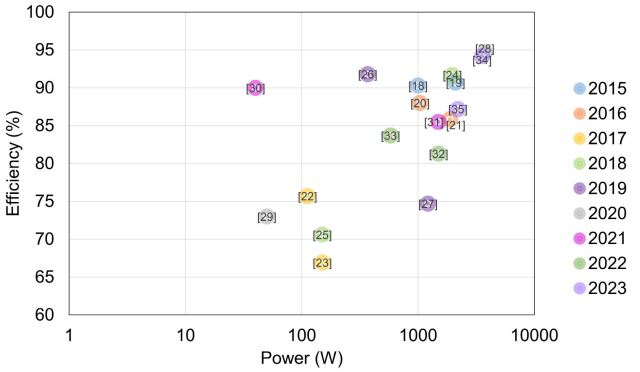

FIGURE 2. System efficiency versus power.

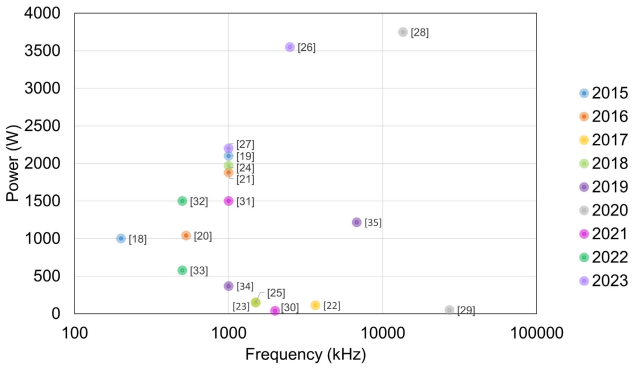

FIGURE 3. Power versus operating frequency.

maritime vessels [9], [10], [11], and unmanned maritime vehicles [12], [13]. In the literature, many papers have reviewed different perspectives on CPT investigating converter topologies, compensation circuits, and structures [3], [4], [14], [15], [16], [17]. However, this paper focuses on surveying a number of published experimental works over the last decade while also discussing the theoretical and practical considerations, challenges, and limitations of designing a CPT system. Additionally, it uses Vector Network Analyzer (VNA) to measure the capacitive coupling parameters. Based on the measurement results, a 13.56 MHz CPT system is designed as a case study. The paper aims to shed light on various aspects of designing a CPT system.

II. SURVEY OF CPT DEVELOPMENT

Although Nikola Tesla firstly demonstrated WPT using capacitive coupling as early as 1891, research on CPT did not receive significant attention until 2008 [4]. Since then, several experimental works have been conducted to enhance the overall system efficiency and enable power transfer over wide separation distance ranges [18], [19], [20], [21], [22], [23], [24], [25], [26], [27], [28], [29], [30], [31], [32], [33], [34], [35]. Dai and Ludois [4] surveyed the empirical published works in a period between 2008 and 2015, examining relationships between different aspects of CPT systems, such as power, efficiency, frequency, and separation distance. This section extends the survey by examining some of the published works from 2015 to 2023.

Fig. 1 shows the efficiency of the examined CPT systems plotted against the separation distance. The size of the bubbles represents the power levels of the systems. The figure indicates that power transfer has been examined over separation distances ranging from a few millimeters up to 300 mm. However, in the past decade, the focus has been on building CPT systems with separation ranges between 150 mm to 360 mm. These separation distances are suitable for electric vehicle (EV) charging applications, as the ground clearance varies depending on the type and load weight of the vehicle.

The efficiencies of all examined systems are above 65%. Systems that transfer kilowatt power levels can achieve high efficiencies, as also shown in Fig. 2. When dealing with kilowatt power levels, it is crucial to have a high-efficiency CPT system; otherwise, a heat dissipation system would be required, increasing the overall system weight and cost. Fig. 1 and Fig. 2 demonstrate that some systems with power around 100 W have an efficiency of less than 80%, but they can operate at wider separation distances exceeding 100 mm. The operating frequency of CPT systems ranges from 200 kHz to 27.283 MHz, as shown in Fig. 3. The Medium Frequency (MF) range, particularly 1 MHz, is the most commonly used operating frequency. Researchers have also managed to transfer kilowatt power levels at High Frequency (HF) operation ranges.

In the last three years, CPT have utilized HF ranges to transfer power levels up to a few kilowatts. Between 2015 and 2023, the researchers have made significant advancements in CPT systems, enabling high-power transfer at high operating frequencies, achieving high efficiency, and supporting wide separation distances. With the continuous advancement of semiconductor switches, it is likely that CPT systems will operate in the High Frequency (HF) range to transfer power over wide separation distances.

III. ELEMENTARY CONSIDERATIONS

This section discusses the fundamental principle of capacitive coupling, the main design factors, and the general structure of CPT system.

A. FUNDAMENTAL OPERATION PRINCIPLE

As previously defined in Section I, CPT transfers power from an electrical power source to an electrical load through alternating electric fields. The fields induce displacement current between the transmitter and the receiver electric circuits. The physical principle of the CPT is embodied in Maxwell's equations which can be presented as

$$\vec{\nabla} \times \left(\vec{\nabla} \times \vec{E} \right) = -\frac{\partial}{\partial t} \left(\nabla \times \vec{B} \right), \tag{1}$$

where E is the electric field (V/m), B is the magnetic field (T). Isolating electric and magnetic fields in (1) gives

$$\vec{\nabla} \left(\vec{\nabla} \cdot \vec{E} \right) - \nabla^2 \vec{E} = -\frac{\partial}{\partial t} \left(\mu\sigma \vec{E} + \mu\varepsilon \frac{\partial \vec{E}}{\partial t} \right), \tag{2}$$

where μ permeability (H/m), σ is the conductivity of the medium Ω/m, and ε is the absolute permittivity of the medium (F/m). The right terms in (2) are the displacement currents corresponding to the time-varying electric displacement fields.

If two conductive plates are uniformly charged with opposite charges distributed over their surface, uniform electric fields are confined between them. However, when the separation distance between the plates is comparable to the dimensions of the plates, the assumption of uniform electric fields is no longer valid, and the fringing effect cannot be neglected. The fringing is the nonuniform distribution and the bending of electric fields near the edges. Several analytical and numerical models tried to calculate the capacitance considering the fringing effects [36]. The fringing fields can couple the plates with the ground or any charged object in proximity, leading to the formation of stray and parasitic capacitors. The stray and other parasitic coupling capacitances significantly impact the design and performance of CPT systems. Besides capacitance, some factors are important in the design of CPT systems.

B. DESIGN FACTORS

The power transferred by a CPT system depends on capacitive coupling, the frequency of the alternating electrical fields, the voltage across the coupling plates, and the phase angle between the voltages and currents in the system. Therefore, the design metrics or factors that influence the overall system performance of a CPT system are [11]:

1) THE CAPACITIVE COUPLING

The capacitance depends on the geometries of the plates, the distance between the couplers, and the medium characteristics between them. The plate thickness can negligible affect the coupling [24]. But it should be considered for accurate design depending on the side-by-side distance between the adjacent plates and the separation distance between the transmitter and the receiver sides. Various geometric configurations were adopted for CPT coupling structures, namely, conventional rectangular shape, cylindrical [37], disk [37], and matrix platform [38]. The coupling factors of these structures widely vary, where the rectangular factor is higher than 0.95, whereas the disk shape is less than 0.5 [37]. The matrix structure gives freedom of movement, but it suffers from low efficiency and may require complex control techniques.

A large surface area of the plates causes an increase in the capacitance, a reduction in the electric field, and a reduction in the fringing effect. However, vast areas can be a challenge to realize in practice. The separation distance between the couplers is another factor that affects the value of the coupling capacitance. If the transmitter and the receiver couplers are farther apart, the effective coupling drastically decreases, and the system is said to be ''loosely coupled.''

The electric properties of the separation medium between the transmitters and receivers play a critical role in capacitive coupling. The air is the common medium between the plates for on-road EV charging applications. As the permittivity of the air is about 1.0006 times the permittivity of the vacuum (i.e., $\varepsilon_0 \approx 8.85 \times 10^{-12}$ F/m), the air-gapped coupling capacitance is in the pF range. Inserting a material layer with a high dielectric between the couplers instead of air enhances the coupler's capacitance.

Researchers proposed the vehicle's wheels [39], windows [40], or bumper [4] to minimize the air gap and confine the field during charging. Water or air can be a separation medium for maritime charging applications between the CPT couplers. Unlike air, the permittivity of water is about 80 times higher than that of air. It depends on the characteristics of water, such as salinity and temperature. The salinity of seawater can increase the coupling capacitance. But it also causes a dielectric loss that degrades the overall efficiency of the system [12], [13], [36].

2) THE OPERATING FREQUENCY

Operating at a higher operating frequency can result in improving the overall energy density of the system and the capability of increasing the distance of power transfer between the couplers. Operating frequency ranges from MF to HF were proposed in the literature, as previously shown in Fig. 3. In the MF ranges, 200 kHz [18], [41] and 848 kHz [42] were used but over air-gapped separation distance of less than 1 mm. Higher frequencies in the MF ranges were also proposed such as 1 MHz [43], 1.5 MHz [25], and 2 MHz [44]. In the HF ranges, 3.4 MHz [45], 6.78 MHz [46], 13.56 MHz [47] and 27.12 MHz [29]. But, high operation frequency can cause high losses and complicate the design and controlling processes.

3) THE VOLTAGE ACROSS COUPLERS

The power transfer is proportional to the voltage squared, and it also depends on the phase shift between the voltage across the couplers and the induced current flows through the circuit nodes. Thus, if a high voltage is applied across the couplers, electric fields increase, and more energy can be transferred. A wide variation of compensation networks helps achieve

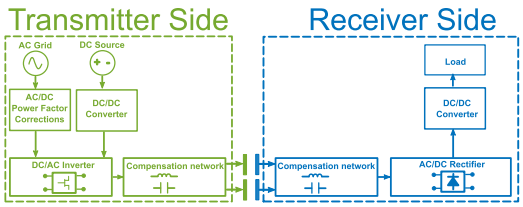

FIGURE 4. Block diagram of a general structure of a CPT system.

high voltage levels and compensates the phase shift between the voltage and current to achieve high power transfer. The compensation networks can be categorized based on the resonation principle, where each category has pros and cons [5]. Isolating transformers can also be used to isolate, compensate and boost the voltages [48].

When the separation medium between the couplers is the air, the coupling capacitance is in pF range, and the voltage across the couplers can reach hundreds or thousands of volts. Applying a very high voltage across the couplers may result in arcing or even a breakdown voltage fault. It also requires expensive components for the compensation circuits that can withstand high voltage ranges. Besides, increasing the voltage increases the electric field between the plates and the fringing field intensity field, which may exceed the safety requirements of the human body.

C. GENERAL SYSTEM STRUCTURE

A block diagram of a CPT for charging applications is shown in Fig. 4. The power source can be an ac grid, a dc grid, a battery unit, or a hybrid combination of ac and dc sources. The connection to an ac grid can face harmonics and power factor challenges due to the nonlinear behavior of the power electronics interface. Thus, the connection should comply with the international standard, IEC 61000-3-2, which prescribes the maximum amplitude of the line frequency harmonics [49].

Passive filters or front-end ac-dc converters are needed to correct the power factor and minimize the current harmonics. Whereas the passive filters comprise bulky components and cannot regulate the power flow and output voltage levels, front-end converters suppress the harmonic contents and control the power flow actively. Various bridgeless converters are proposed for power factor correction applications [50], [51] that can be an attractive option for a CPT charging system. In contrast, connecting to a dc grid or batteries requires dc-dc converters to step up or down the source voltage to the required input voltage for the CPT system.

Capacitive coupling is the essential part that transfers between electrical networks by means of electric fields. Various arrangements of plates to form capacitive couplers were proposed, as illustrated in Fig. 5. The two-plate arrangement is a quasi-CPT, proposed to simplify the capacitive coupling structure, where the ground forms the common return path [52]. In this structure, the stray capacitance between the chassis of EV and the ground provides a return path that

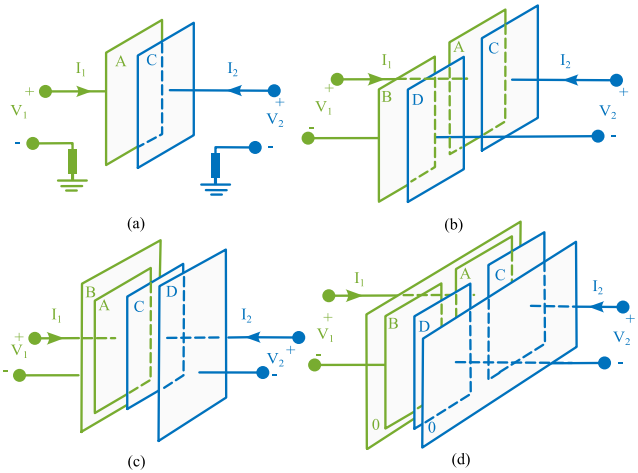

FIGURE 5. Capacitive couplers structure: (a) A Two-plate structure [52]. (b) A four-plate horizontal structure [19]. (c) A four-plate vertical structure [21]. (d)A six-plate structure [24], [46], [53].

can result in dangerous high voltage variation on the vehicle chassis and Electromagnetic Interference (EMI) problems.

The four-plate horizontal structure is the most commonly used and tested in the literature [19]. Compared to the four-plate horizontal structure, the four-plate vertical structure was proposed as a more compact arrangement to save space [21]. But the size of plates B and D should be larger than that of plates A and B. Finally, the six-plate recently received more attention, a four-plate horizontal structure with two extra plates shielding the electric field and expanding the safety area [24], [46], [53].

Compensation circuits are required to achieve Zero Phase Angle (ZPA) reducing the reactive power and increasing the active power transferability. Double-sided symmetrical compensation typologies, including L, LC, LCL, LCLC, CLLC compensations, were commonly used [7]. Other researchers proposed a single-sided primary compensation [43], [46], [53]. Although the compensation for a capacitive coupling can be applied on the transmitter side only, an impedance-matching network is required at the secondary side to achieve high efficiency over a wide load variation.

The configuration of compensation circuits depends on the type of input and output of the resonant circuits. For instance, a T-circuit configuration is required to have a constant-voltage output. In contrast, a π-circuit configuration is required to achieve a constant-current output for a constant-voltage input of the compensation circuits [15]. Increasing the resonant components in the compensation circuits will increase the overall cost of an CPT system and the difficulties of the design and realization in practice.

The compensation or impedance-matching network on the receiver side is followed by an ac-dc rectifier which converts the received alternating power to constant power. Following the rectifier, a dc-dc converter is required to keep the effective output load of the rectifier close to the optimal load. The dc-dc converter is needed to connect to a dc grid or batteries.

It adjusts the output voltage to the required voltage level and can be operated as active impedance matching.

IV. THEORETICAL CONSIDERATIONS

Operating in MF to HF, the corresponding electromagnetic wavelength will range from tens to hundreds of meters, making the lumped circuit element approximations of circuit theory valid. The network theory would help bridge the gap between field analysis and circuit theory. Thus, this section presents some of the elements of the network theory that are useful in the study of CPT systems. It discusses the main concepts, the fundamental principles, and the basic elementary network theorems based on the details in [54] and [55].

The physical principles of the network theory are embodied in Maxwell's equations, as expressed in (2). Thus, the network theory follows two main physical principles.

The first principle is the linearity principle, which is based on the linearity of Maxwell's equations. A CPT system can be modeled as a linear two- or multi-port network, characterized by using a number of linear impedance elements, which are passive elements with two terminals. Capacitance and inductance are impedance element values that describe the lossless operation of a network and represent the flow of energy in the form of electric and magnetic fields. The resistance and conductance are the impedance element values that represent the losses in the network.

The second principle is the duality principle, resulting from Maxwell's equations' symmetries. The duality gives great convenience in analyzing WPT systems. Based on this principle, IPT systems can be considered dual for CPT systems. For instance, a IPT system can be modeled as a black box that contains a network of impedances. In contrast, a CPT system can generally be modeled as a black box with a network of admittances.

Four network theorems are helpful for WPT analysis: superposition, reciprocity, Thevenin/Norton, and bisection theorems. The superposition theorem follows directly from the linearity of Maxwell's equations. It states that if more than one source is present in a linear bilateral network, the response across any element in the network is the sum of the responses obtained from each source separately. The reciprocity theorem, which follows the symmetry of Maxwell's equations, states that the admittance and impedance matrices are symmetrical. However, this theorem fails if the network contains active devices or nonreciprocal mediums (e.g., Ferrites). Norton's (Thevenin's) theorem states that any network having two accessible terminals can be simplified to an equivalent circuit consisting of a single current source (a single voltage source) and parallel admittance (series impedance) that is connected to a load. Finally, the bisection theorem states that if equal voltages are applied to the terminals of a symmetrical network, no current will flow across the symmetrical components.

A capacitive coupler is an electrical network with one or more impedance elements connected at nodes forming electric meshes. If the impedance elements are known, then

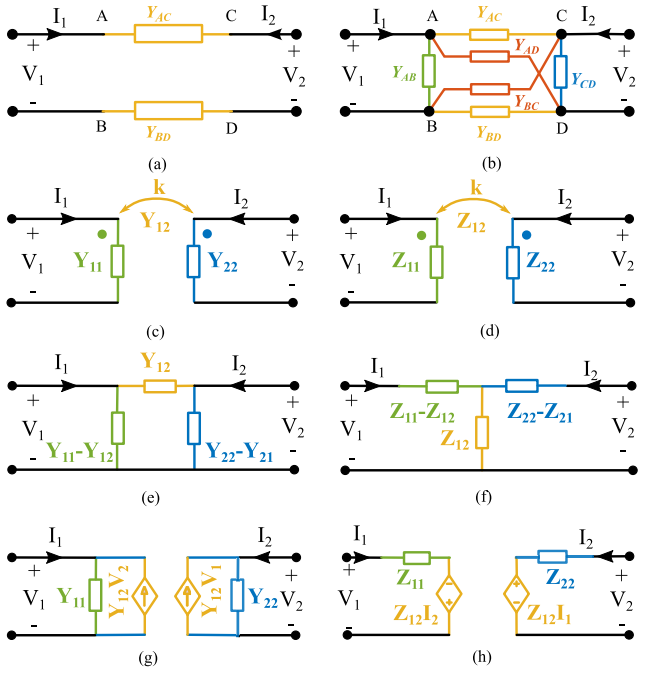

FIGURE 6. Capacitive couplers: (a) Theoretical coupling admittances. (b) Mutual-, self-, and cross-coupling admittances. (c) Circuit current type model. (d) Circuit voltage type. (e) Circuit equivalent π- network model. (f) Circuit equivalent T-network model. (g) Behavior current-source model. (h) Behavior voltage-source model.

the current flows into, and the voltages applied on a network can be found using the law of conservation of energy and the law of conservation of charge (i.e., Kirchhoff's voltage law and Kirchhoff's current law, respectively). Using these two laws, the mesh currents can be expressed as a function of the applied voltages in a mesh. Various electrical network configurations were proposed to model the capacitive coupling between plate structures. Theoretically, capacitive couplers can be modeled considering the medium losses using coupling admittance, as illustrated in Fig. 6 (a). In practice, however, three types of coupling can exist (1) effective-coupling (Y_{AC} and Y_{BD}), (2) cross-coupling (Y_{AD} and Y_{BC}), and (3) self-coupling (Y_{AB} and Y_{CD}), as shown in Fig. 6 (b).

An ideal voltage or current transformation can be used to model these coupling admittances, which are equivalent to a transformer model, as in Fig 6 (c) and (d), respectively. In these models, the admittance Y_{12} or the impedance Z_{12} are equivalent to the mutual coupling in an electromagnetic network, while the admittances Y_{11} and Y_{22} or the impedances Z_{11} and Z_{22} are equivalent to the leakage or the stray coupling to the ground.

Using the concept of the electrical network, the voltages and currents in the network can be considered unknown variables, which can be obtained using a simple set of equations. Fig 6 (e) shows the circuit equivalent π-network model, which is the most common model used to model CPT systems in the literature. The circuit equivalent T-network model is mainly used in modeling IPT. Still, it can be used to model CPT systems using the duality principle [41], [56],

as illustrated in Fig 6 (f). Behavior source models are other approaches to represent WPT system. Fig. 6 (g) shows the behavior current-source model, which is the most commonly used in CPT [24], [52]. The behavior voltage-source model has recently attracted more attention in CPT analysis [41], [56], as shown in Fig. 6 (h).

All the models presented in Fig. 6 are 2-port models. The models shown in Fig. 6 (d), (f), and (h) are proposed to compare magnetic field coupling to electric field coupling. However, the models in Fig. 6 (c), (e), and (g) are closer to the actual capacitive coupling system. The calculated or measured values of the coupling admittance can be implemented directly into these models.

Mathematically, the π-network model can be expressed as

$$Y_{11} - Y_{12} = Y_{AB} + \frac{(Y_{AC} + Y_{AD}) \cdot (Y_{BC} + Y_{BD})}{Y_{AC} + Y_{AD} + Y_{BC} + Y_{BD}} \tag{3}$$

$$Y_{22} - Y_{12} = Y_{CD} + \frac{(Y_{AC} + Y_{BC}) \cdot (Y_{AD} + Y_{BD})}{Y_{AC} + Y_{AD} + Y_{BC} + Y_{BD}} \tag{4}$$

$$Y_{12} = \frac{Y_{AC} \cdot Y_{BD} - Y_{AD} \cdot Y_{BC}}{Y_{AC} + Y_{AD} + Y_{BC} + Y_{BD}} \tag{5}$$

If the impedance elements are known, the current flows into, and the voltages applied on a network can be found using Kirchhoff's voltage and current laws. The voltage and current on the transmitter side can be expressed as a function of the voltage and current on the receiver side as follows.

$$\begin{bmatrix} V_1 \\ I_1 \end{bmatrix} = \begin{bmatrix} A & B \\ C & D \end{bmatrix} \begin{bmatrix} V_2 \\ I_2 \end{bmatrix} \tag{6}$$

$$= \begin{bmatrix} \frac{Y_{22}-Y_{21}}{Y_{12}} & \frac{1}{Y_{12}} \\ \frac{(Y_{11}-Y_{12})(Y_{22}-Y_{21})-Y_{12}^2}{Y_{21}} & \frac{Y_{11}-Y_{12}}{Y_{21}} \end{bmatrix} \begin{bmatrix} V_2 \\ I_2 \end{bmatrix} \tag{7}$$

The determinant of the matrix is unity. For a lossless CPT system, A and D are purely real, and B and C are pure imaginary values if the CPT system is symmetric (i.e., $Y_{12} = Y_{21}$), then $A = D$. This representation is more convenient when the capacitive two-port network is cascaded with other networks, such as the compensation circuits.

If a 2-port network is connected to a current source (I_s and Y_s) and an arbitrary load Y_L, as shown in Fig. 7 (a). Then, the input admittance Y_{in}, as seen watching from the source side is expressed as [57]

$$Y_{in} = Y_{11} - \frac{Y_{12}^2}{Y_{22} + Y_L} \tag{8}$$

The source circuit can be replaced by its Norton equivalent, as illustrated in Fig. 7 (b), and expressed as

$$Y_{out} = Y_N = Y_{22} - \frac{Y_{12}^2}{Y_{11} + Y_S}, \tag{9}$$

$$I_N = \frac{-Y_{12}}{Y_{11} + Y_S} I_s. \tag{10}$$

The degree of coupling between the transmitter and the receiver side is the coefficient of coupling and can be

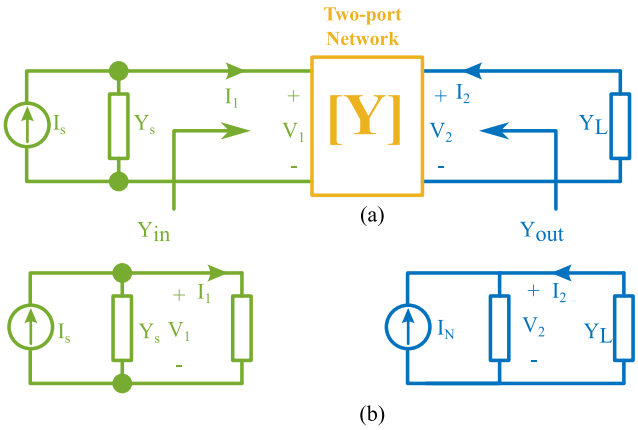

FIGURE 7. A general representation of CPT system connected to a source and a load: (a) Two-port network connected to a source and an arbitrary load. (b) The equivalent circuits use Norton's theorem.

expressed as

$$k = \frac{Y_{12}}{\sqrt{Y_{11} \cdot Y_{22}}} \tag{11}$$

This parameter ranges from negative unity to unity, where the negative represents the phase inversions.

Corresponding to the admittance matrix is the scattering matrix, which comprises the scattering parameters, also known as "s-parameters". Researchers have used the s-parameters to analyze CPT systems [12], [58], [59]. The admittance Y matrix is related to the scattering matrix S by

$$Y = \frac{1}{50} \cdot (E + S)^{-1} \cdot (E - S) \tag{12}$$

where E is the identity matrix, 50 Ω is the reference resistance, and $S = \begin{bmatrix} S_{11} & S_{12} \\ S_{21} & S_{22} \end{bmatrix}$ is the scattering matrix.

Accurate determination of coupling parameters is essential in designing a CPT system. Some researchers use Finite Element Method (FEM)-based software [21], [24], [52] to calculate the coupling between the plates, or they measure the parameters using impedance analyzer [36], [46], [47], [53]. Other researchers [12], [13], [57], [59] use VNA to utilize the s-parameters directly. Calculating or measuring the coupling parameters requires accurate modeling. The next section introduces some practical considerations for finding these parameters.

V. PRACTICAL CONSIDERATIONS

Selecting the required compensation and optimizing the efficiency of the system depends on accurately measured or calculated capacitive coupling parameters. Usually, FEM-based software calculates the coupling capacitance between the plates. Calculating the capacitances between several plates is achieved by calculating the charge of any plate and the electrostatic potentials on all other plates. The relations between the charge of the i^{th} plate to the voltages of all plates in the system are described by the Maxwell capacitance matrix [60]. The diagonal elements of his matrix C_{ii} are determined by

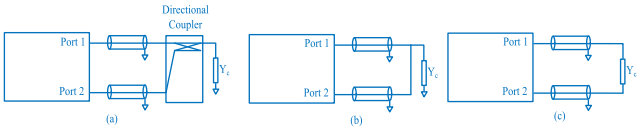

FIGURE 8. Types of measurement techniques: (a) Reflection, (b) Shunt-through. (c) Series-through.

calculating the charge on the i^{th} plate when only the voltage is applied to this plate and other plates are grounded. Thus, the diagonal elements are the addition of the self-capacitance (i.e., the stray or parasitic capacitance between the plate to infinity) and the mutual capacitances (i.e., the capacitances due to the potential differences between the plates).

The Maxwell capacitance matrix is calculated numerically by solving the electrostatic potential, which depends on the boundary condition. In Ansys Maxwell©, the boundary condition is floating at infinity in which a matrix reduction operation is applied within a margin of error [61]. In this condition, the boundary is disconnected from the ground at infinity and assumed as it is a perfectly conducting surface over which the potential is constant. The condition implies that the electric fields are perpendicular to the boundary. Another approach is the zero charge boundary condition which assumes that the electric field lines are tangential to the boundary. In this condition, the boundary is assumed to be a perfectly insulating surface through which the charge cannot redistribute itself. COMSOL Multiphysics© can apply both conditions and take the average of the two is sufficient for practical application [62].

The coupling parameters can be measured using either an impedance analyzer or VNA. An impedance analyzer is a four-terminal device that uses the I-V method (i.e., a current source and sensitive voltmeter) to measure the impedance over a wide frequency range accurately. It has excellent measurement stability after calibration, but test fixture stray impedance and admittance need to be accurately eliminated [63]. In contrast, VNA is a device that has one, two, or four ports that use s-parameters to measure the impedance over a frequency range from a few hundreds of hertz to GHz. It requires calibration each time the instrument is turned on or the frequency setting is changed [63]. However, the calibration parameters can be stored and reloaded each time they are required. A check on the validity of such calibration should be performed from time to time. Both devices should give results that agree with each other within the uncertainty in a frequency range from 30 kHz to 100 MHz [64].

Several measurement techniques can measure the coupling parameters using VNA: reflection, shunt-through, series-through, π-network, and the I-V method [63]. Fig. 8 illustrates the reflection, shunt-through, and series-through techniques.

The reflection technique requires one port only to achieve the measurements, as it uses the reflection coefficient by measuring the ratio of the incident signal and reflected signal (i.e., $\Gamma = {}^{V_r}/_{V_i}$). The admittance can be calculated from the reflection coefficient as

$$Y_c = \frac{1}{50} \cdot \frac{1-\Gamma}{1+\Gamma} \tag{13}$$

The directional coupler measures the reflected signal at a null balance point. Thus, this technique gives accurate results if the measured impedance is close to or equal to the device reference impedance (50 Ω).

The shunt-through technique requires two ports. The couplers are connected parallel to the two ports, and the measurements can be calculated using the following expression.

$$Y_c = \frac{2}{50} \cdot \frac{1-S_{21}}{S_{21}} \tag{14}$$

This technique is more suitable for high admittance measurements since it depends on the transmission coefficient.

The series-through technique requires two ports. The couplers are connected in series to the two ports, and the measurements can be calculated using the following expression.

$$Y_c = \frac{1}{2 \cdot 50} \cdot \frac{S_{21}}{1-S_{21}} \tag{15}$$

This technique is more suitable for low-admittance measurements as it depends on the reflection coefficient but is still sensitive to calibration uncertainty.

The series-through can measure the coupling capacitance between using a one-port of VNA. Measurements can be modeled using the π-network model for capacitive coupling. Previously, the VNA has been used to measure the coupling admittance [12], [13], [57], [59]. The ports of the VNA are connected to the two plates of the coupler, while the other plates are connected to the ground of the VNA. For a shielded CPT system, the shield plates should also be connected to the ground of the VNA, as shown in Fig. 9. For instance, the effective-coupling admittance between plates A and C is modeled as Y_{AC}, as illustrated in Fig. 9. The stray admittance Y_{AC0} models the leakage admittances to the ground and the parasitic coupling with other plates.

One-port of VNA can measure the capacitive coupling. Using the short-circuit and open-circuit approaches, shown in Fig. 9(b), the effective-coupling admittance and its stray capacitance can be expressed as

$$Y_{sc} = Y_{AC0} = Y_{AC0} \tag{16}$$

$$Y_{oc} = Y_{AC0} - \frac{Y_{AC}^2}{Y_{AC0}}, \tag{17}$$

where $Y_{AC0} = g_{AC0} + j\omega C_{AC0}$ models all the stray and parasitic addmitances. In the air-gapped shielded CPT system, the conductivity (i.e., the real part of the admittance) is negligible. Then the capacitances can be calculated directly from the imaginary part of the admittances.

The two-port of VNA can also measure the capacitive coupling. Fig 9(c) shows the measurement can be achieved using the two-port of the VNA. The two-port approach can achieve the measurement in one step compared with the one-port approach, which requires two measurement steps. The

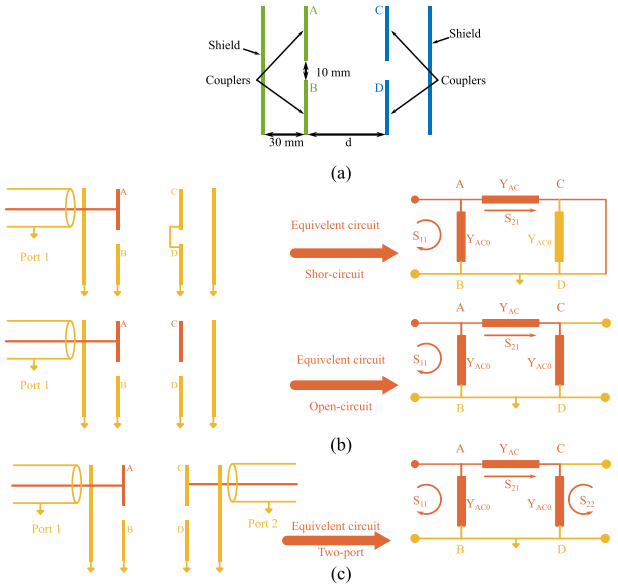

FIGURE 9. Shielded CPT: (a) Physical dimensions. (b) One-port measurement approach. (c) Two-port measurement approach.

admittances can be measured using the two-port as follows

$$Y = \frac{1}{Z_0}(E - S)(E + S)^{-1} \tag{18}$$

$$= \begin{bmatrix} Y_{AC} + Y_{AC0} & -Y_{AC} \\ -Y_{AC} & Y_{AC} + Y_{AC0} \end{bmatrix}, \tag{19}$$

where $Z_0 = 50\Omega$ is the reference impedance, E is the identity matrix, and S is the s-parameter matrix that achieved from the measurements.

VI. CASE STUDY: DESIGN A 13.56 MHz CPT SYSTEM

This section describes the design and measurement of a shielded CPT system operating at a frequency of 13.56 MHz. The system composes four 150 × 250 mm plates which form the couplers (A, B, C, and D), and two 250 × 300 mm shield plates. The distance between the adjacent plates (i.e., AB or CD) is 10 mm, and the distance between the couplers and shields is 30 mm, as shown in Fig. 9(a).

The coupling parameters can be measured using the one- and two-port approaches discussed in section V. Using the one-port approach, the effective-coupling capacitance can be calculated using the short-circuit and open-circuit techniques, as illustrated in Fig. 9 (b). In contrast, the parameters of the π-network model are directly achieved from (19) using the connection shown in Fig. 9(c). Similarly, the cross-coupling between plates A and D or B and C can be measured using the aforementioned approaches.

Fig. 10 shows the measured and simulated changes in the effective- and cross-coupling capacitances with varying separation distances. The calculated values are achieved using the equation $C = {}^{\varepsilon A}/_{d}$, the simulated values are given by COMSOL Multiphysics©, and the measured values are achieved using both one- and two-port approaches. The one-port measurements provide close values to the calculated ones, while the two-port measurements give close values

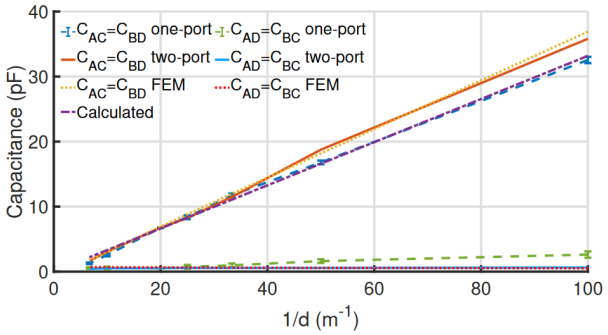

FIGURE 10. Calculated and measured values of effective and cross-coupling coupling capacitance.

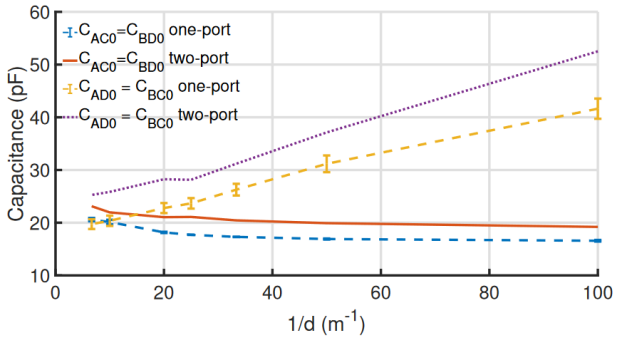

FIGURE 11. Measured values of stray capacitance.

to the simulated ones. The difference between the one-port and two-port measurements is attributed to the high stray capacitance values at short separation distances, which can introduce calculation errors in the one-port approach.

Fig. 11 shows the stray capacitances for both the effective and cross-coupling cases. The stay capacitances have higher values compared to effective and cross-coupling capacitances. The stray capacitance of the effective coupling (Y_{AC0} or Y_{BD0}) mainly composes the self-coupling capacitance and the parasitic capacitance between the plates and shields. Thus, it merely changes when the separation distance between the plates is increased. In contrast, The stray capacitance of the cross-coupling (Y_{AD0} or Y_{BC0}) mainly composes of the stray capacitance between A and C. Thus, it decreases when the separation distance is increased.

Compared to the reflection, shunt-through, and series-through measurement techniques, the one- and two-port methods can directly measure the stray admittances. As the series-through technique has a similar connection configuration to the one- and two-port techniques, Table 1 presents the measured coupling parameters at a separation distance of 30 mm. The series-through, one-port, and two-port techniques are compared, showing that the two-port technique provides closer results to the simulated values. The series-through technique gives closer results to the two-port technique, but additional measurement steps are required to measure the stray capacitance. The one-port technique is less accurate, especially for cross-coupling capacitances (C_{AD} and C_{BC}), due to calculation errors resulting from

TABLE 1. The measured coupling parameters at 30 mm separation distance.

Coupling parameters	Series-through	One-port	Two-port
C_{AC} (pF)	11.5842	11.7408	11.4761
C_{BD} (pF)	11.4386	11.1282	11.3322
C_{AD} (pF)	0.5743	0.975	0.5684
C_{BC} (pF)	0.5778	0.9302	0.5778
C_{AB} (pF)	11.5842	11.1982	11.3322
C_{CD} (pF)	11.4386	11.7465	11.4761
C_{AC0} (pF)	–	17.3115	21.1783
C_{AD0} (pF)	–	26.2693	31.1869
C_{AB0} (pF)	–	22.5022	25.7621

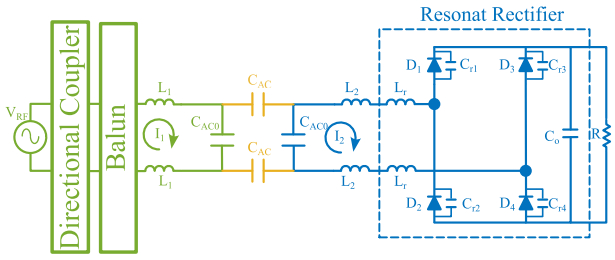

FIGURE 12. A schematic of the 13.56 MHz CPT system.

high stray capacitance values and losses/discontinuities in the connections.

The effective coupling capacitances and the stray capacitance are the main design factors. While the distances between the plates and the shields and between the adjacent plates affect the stray capacitance, the separation distance between the transmitter and receiver couplers affects the effective coupling. In practice, the plate D is not connected to the ground, resulting in a π-network model similar to the one shown in Fig. 12. The figure illustrates the schematic of the proposed CPT system. An RF generator (Advanced Energy RFX600A) generates a 13.56 MHz ac power. A Ruthroff balun is connected to the shield plate to achieve a stable ground level. An RF Wattmeter (LP-100A Digital Vector) is used to measure the input ac power to the system, and a Tektronix TPS2014b oscilloscope measures the output voltage.

At a 30 mm separation distance, the design parameters are listed in Table 2. Based on the theoretical and practical procedure, Fig. 13 illustrates the flow chart to design the proposed CPT system. The operating frequency is an important factor in designing a CPT system. The separation distance between the plates affects the power transfer capability, as well as the distances between adjacent plates and plates/shields. These distances determine the coupling parameters of the system. The series compensation is a simple configuration that is used to enhance the overall efficiency, reduce the reflected power, and achieve ZPA operation condition. The inductance should compensate for both the stray and coupling capacitance. The inductor is split into both transmitter and receiver sides to eliminate any leakage current flows through stray capacitances. The compensation inductances can be calculated as [65]

$$L_1 = L_2 = \frac{1}{2\omega_0^2} \frac{C_{AC0}}{C_{AC0}^2 - \left(\frac{C_{AC}}{2}\right)^2}, \tag{20}$$

TABLE 2. Design parameters.

Symbol	Quantity	Value
f	Operating frequency	13.56 MHz
d	Separation distance	30 mm
C_{AC}	Effective coupling capacitance	11.5 pF
C_{AC0}	Stray capacitance	20.6 pF
L_1 & L_2	Compensation inductance	3.6 µH
$C_{r1}, C_{r2}, C_{r3}, C_{r4}$	Resonant capacitance	63.1 pF
L_r	Resonant inductance	1 µH
R	Load resistance	400 Ω
D_1, D_2, D_3 & D_4	Diode of the rectifier	GD30MPS12H

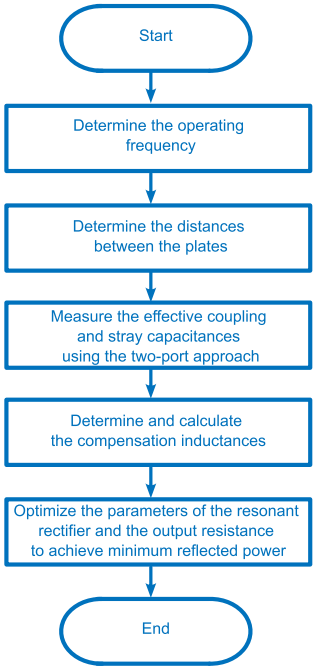

FIGURE 13. A flow chart to design a HF CPT system.

where ω_0 is the angular resonant frequency. Symmetrical compensations on each side are used to achieve stabilized ground voltage.

The resonant rectifier circuit is used to achieve DC output and minimize reflected power. The components of the resonant rectifiers are optimized using LTspice© for minimum reflected power [68]. Reflected power is an important factor to achieve an efficient CPT. Minimizing the reflected power maximizes the forward transferred power and the overall system efficiency. According to [68], the proposed system can achieve minimum reflected power at a 400 Ω load resistance, 63.1 pF resonant capacitance connected parallel to the diodes, and 1 µH series-compensated resonant inductance. The series-compensated resonant inductors of the rectifiers can be integrated into the series inductors of the CPT system to reduce the number of components.

Fig. 14 depicts the proposed CPT system under test. The proposed system transfer 100 W input power at an 87.4% efficiency and 187 V output voltage. The efficiency is calculated from the measured output voltage and input power $V^2/(R \cdot P_{in})$. Fig. 15 shows the testing results in which the input voltage is in phase with the input current resulting in minimum reflected voltage. Combing the parasitic resistances of the inductors,

TABLE 3. Comparison between the proposed CPT system and other HF CPT systems in the literature.

Ref.	Plates No.	Power (W)	Efficiency (%)	Frequency (MHz)	Distance (mm)	Size (mm)
[27]	4	590	88.4	6.78	120	122.5 × 122.5
[66]	4	100	83.5	6.78	12	100 × 100
[67]	4	122.9	73.6	16.5	1	100 × 100
[29]	8	50	73	27.12	250	10ϕ & 25ϕ
This work	6	100	87.4	13.56	30	250 × 150 and 250 × 300

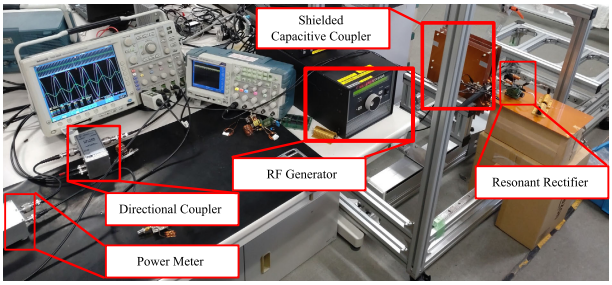

FIGURE 14. The CPT system undertest.

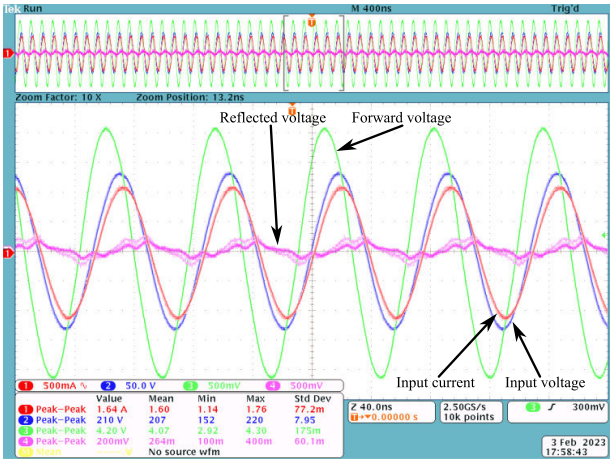

FIGURE 15. The waveform results.

the Balun circuit, and the on-resistance of the diodes in the rectifier increase the matching network losses and hence the reflected voltage.

Table 3 presents a comparison of this work with other HF CPT systems in the literature in terms of the number of plates, transfer power, system efficiency, operating frequency, transfer distance, and coupler size. The matching network system proposed in [27] is determined using the optimization approach resulting in a higher efficiency system over a wider separation distance compared to the proposed one. The system proposed in [66] transfers the same power level as the proposed system but over a shorter separation distance and lower efficiency. The paper [29] proposes a three-phase CPT system which can operate at wide separation distances and a high operating frequency.

This work proposes a shield CPT system is shielded to reduce the EMI problem and increase the safety around the couplers. Although the system transferred 100 W at an efficiency of over 87.4% at 30 mm separation distance, it can operate at higher power than 100 W. Edgewise coils can be used to build up the compensation circuits and decrease the parasitic losses, but it will also increase the cost of the system.

VII. DESIGN LIMITATIONS AND CHALLENGES

This section discusses design challenges, including operating frequency, voltage stress, stray capacitance and ground stability, and overall system efficiency.

A. OPERATING FREQUENCY

The operating frequency of CPT systems, unlike IPT systems, have not been standardized since these systems are still under testing in laboratories. Generally, frequencies in the medium to high-frequency range are adapted for transferring power ranging from hundreds of watts to a few kilowatts. Operating at high frequency adds an extra challenge to designing and tuning circuits in practice. Besides, if the intensity of the fields exceeds the limits, they can induce electric fields in exposed bodies, leading to issues such as tissue heating or nerve stimulation. The International Commission on Non-Ionizing Radiation Protection (ICNIRP) [69] specifies the basic restriction for the electric field exposure from 100 kHz to 10 MHz for any region of the human body by the following

$$E_{\text{ind}} = 2.7 \times 10^{-4} f, \quad \text{Occupational} \tag{21}$$

$$E_{\text{ind}} = 1.35 \times 10^{-4} f, \quad \text{General public} \tag{22}$$

where E_{ind} the induced electric fields (V/m) and f is the operating frequency (Hz). These restrictions help ensure safety by limiting the induced electric fields within acceptable levels. It is important to carefully consider and adhere to these safety guidelines when designing and operating CPT systems, particularly when operating at higher frequencies where the risks associated with induced electric fields are more pronounced.

B. VOLTAGE STRESS

The induced fields are directly related to the voltage stress across the couplers. Increasing the voltage stress would require higher safety clearances around the coupling plates to prevent the induced electric fields from exceeding the specified limits. The voltage across the plates in a CPT system can reach several kilovolts to effectively transfer power effectively over a few hundreds of mm. As the breakdown voltage of the air is 3 kV/mm, this limits the distances between the plates to avoid arcing or breakdown faults. In a non-shielded CPT system, operating with high voltage stress

not only increase the safety clearness around the system but also introduces the risk of inducing voltage on the metallic body of the vehicle or nearby objects through stray capacitors. This increases the potential for electric shocks if there is any contact with these objects.

In a shielded CPT system, the shields can contain electric fields providing a level of protection and decreasing the range of the safety clearance from the plates. However, it still has limitations concerning the compactness of the system due to the high voltage stress. Operating frequency at 13.56 MHz and a separation distance of 180 mm, the shielded-CPT coupling structure requires about 30 mm gap between the shields and the couplers to maintain safety and prevent breakdown or arcing [70]. To mitigate the challenges associated with high voltage stress, several voltage stress optimization methods have been proposed in the literature. These methods aim to reduce the voltage stress across the couplers minimizing the risks associated with high voltage stress. Some of these methods can be found in [41], [71], [72], and [73].

C. STRAY CAPACITANCES AND GROUND STABILITY

The electric fields are divergent, terminating between any two electrodes with potential differences. Because of the potential difference between the coupling plates and the ground resulting in stray capacitances, which can be a source of EMI. Besides, the leakage fields around the plates can couple with any low electric potential objects, which raises safety issues. The shielded CPT [24], [46], [53], using a six-plate structure shown in Fig.5 (d), results in a small field leaking out to the surroundings, and it decreases the safety range to about 100 mm away from this plates. However, the coupling between the shielding plates and the ground through the stray capacitances results in an unbalanced ground of the CPT. This unbalanced ground can cause stability issues and affect the system's performance. To address this, the Ruthroff transmission line transformer balun can tackle the unbalanced ground of the shielded CPT and enhance the stability of ground level at the shield plate [74].

D. EFFICIENCY

The efficiency of the coupling capacitance is a function of the coupling parameters. Any change in these parameters might result in a degradation of the overall efficiency. For instance, by increasing the separation distance or introducing any interference of objects between the couplers can directly degrade the overall system efficiency [75]. Operating in the HF range is another challenge for the CPT systems. Soft-switching in both the inverter and rectifier is required to achieve low losses. Impedance matching circuits are also required to enhance the overall system efficiency and power transferability, but they also contribute to some of the overall losses in the system.

The design and optimization of CPT systems require careful consideration of various factors, including voltage stress, safety clearances, compactness, efficiency, and EMI to ensure reliable and safe operation. By employing a shielded CPT system and utilizing techniques such as the transmission line transformer balun, it is possible to mitigate EMI issues, reduce field leakage, and enhance the stability of the system's ground level. Overall, designing an efficient CPT system involves careful consideration of coupling parameters, interference mitigation, soft-switching techniques, and impedance-matching circuits. Balancing these factors is crucial to achieving high efficiency and effective power transfer.

VIII. CONCLUSION

This paper provides an overview and discussion of the theoretical and practical considerations in designing a CPT system. It surveys a number of empirical published works between 2015 and 2023, highlighting the fundamental operating principles and theoretical/practical considerations for designing a CPT system. The coupling parameters are typically determined through numerical calculations using the FEM simulations or by measuring the S-parameters using a VNA. The paper specifically examines the use of one- or two-port VNA measurement techniques for determining the coupling admittances. The two-port approach is generally more accurate than the one-port approach. Based on the two-port measurement results, the paper presents the design of a 13.56 MHz CPT system that achieves the transfer of 100 W with an efficiency of 87.4% at a separation distance of 30 mm. Finally, the paper highlights some design limitations and challenges associated with CPT systems. These challenges include voltage stress and breakdown issues, stray capacitors and ground stability, and overall system efficiency. Further research is needed to address these challenges and improve the performance of CPT systems.

REFERENCES

[1] ITU-R Recommendation ITU-R SM.2110. (Nov. 9, 2021). *Frequency Ranges for Operation of non-Beam Wireless Power Transmission Systems*. [Online]. Available: https://www.itu.int/rec/R-REC-SM.2110-0-201709-S
[2] T.-C. Alicia, G.-G. José, and A. José, *A Wireless Power Transfer for Electric Vehicles: Foundations and Design Approach*. Cham, Switzerland: Springer, 2020.
[3] D. Vincent, P. S. Huynh, N. A. Azeez, L. Patnaik, and S. S. Williamson, "Evolution of hybrid inductive and capacitive AC links for wireless EV charging—A comparative overview," *IEEE Trans. Transport. Electrific.*, vol. 5, no. 4, pp. 1060–1077, Dec. 2019.
[4] J. Dai and D. C. Ludois, "A survey of wireless power transfer and a critical comparison of inductive and capacitive coupling for small gap applications," *IEEE Trans. Power Electron.*, vol. 30, no. 11, pp. 6017–6029, Nov. 2015.
[5] F. Lu, H. Zhang, and C. Mi, "A review on the recent development of capacitive wireless power transfer technology," *Energies*, vol. 10, no. 11, p. 1752, Nov. 2017.
[6] Y. Wang, H. Zhang, and F. Lu, "Review, analysis, and design of four basic CPT topologies and the application of high-order compensation networks," *IEEE Trans. Power Electron.*, vol. 37, no. 5, pp. 6181–6193, May 2022.
[7] M. Z. Erel, K. C. Bayindir, M. T. Aydemir, S. K. Chaudhary, and J. M. Guerrero, "A comprehensive review on wireless capacitive power transfer technology: Fundamentals and applications," *IEEE Access*, vol. 10, pp. 3116–3143, 2022.
[8] A. Ahmad, M. S. Alam, and R. Chabaan, "A comprehensive review of wireless charging technologies for electric vehicles," *IEEE Trans. Transport. Electrific.*, vol. 4, no. 1, pp. 38–63, Mar. 2018.
[9] L. Yang, M. Ju, and B. Zhang, "Bidirectional undersea capacitive wireless power transfer system," *IEEE Access*, vol. 7, pp. 121046–121054, 2019.

[10] H. Zhang and F. Lu, "Feasibility study of the high-power underwater capacitive wireless power transfer for the electric ship charging application," in *Proc. IEEE Electric Ship Technol. Symp. (ESTS)*, Washington, DC, USA, Aug. 2019, pp. 231–235.

[11] H. Mahdi, B. Hoff, and T. Østrem, "Evaluation of capacitive power transfer for small vessels charging applications," in *Proc. IEEE 29th Int. Symp. Ind. Electron. (ISIE)*, Jun. 2020, pp. 1605–1610.

[12] M. Tamura, Y. Naka, K. Murai, and T. Nakata, "Design of a capacitive wireless power transfer system for operation in fresh water," *IEEE Trans. Microw. Theory Techn.*, vol. 66, no. 12, pp. 5873–5884, Dec. 2018.

[13] M. Tamura, K. Murai, and M. Matsumoto, "Design of conductive coupler for underwater wireless power and data transfer," *IEEE Trans. Microw. Theory Techn.*, vol. 69, no. 1, pp. 1161–1175, Jan. 2021.

[14] X. Lu, P. Wang, D. Niyato, D. I. Kim, and Z. Han, "Wireless charging technologies: Fundamentals, standards, and network applications," *IEEE Commun. Surveys Tuts.*, vol. 18, no. 2, pp. 1413–1452, 2nd Quart., 2016.

[15] W. Zhang and C. C. Mi, "Compensation topologies of high-power wireless power transfer systems," *IEEE Trans. Veh. Technol.*, vol. 65, no. 6, pp. 4768–4778, Jun. 2016.

[16] H. T. Nguyen, J. Y. Alsawalhi, K. A. Hosani, A. S. Al-Sumaiti, K. A. A. Jaafari, Y. Byon, and M. S. E. Moursi, "Review map of comparative designs for wireless high-power transfer systems in EV applications: Maximum efficiency, ZPA, and CC/CV modes at fixed resonance frequency independent from coupling coefficient," *IEEE Trans. Power Electron.*, vol. 37, no. 4, pp. 4857–4876, Apr. 2022.

[17] B. Minnaert, F. Mastri, N. Stevens, A. Costanzo, and M. Mongiardo, "Coupling-independent capacitive wireless power transfer using frequency bifurcation," *Energies*, vol. 11, no. 7, p. 1012, 2018.

[18] J. Dai and D. C. Ludois, "Single active switch power electronics for kilowatt scale capacitive power transfer," *IEEE J. Emerg. Sel. Topics Power Electron.*, vol. 3, no. 1, pp. 315–323, Mar. 2015.

[19] F. Lu, H. Zhang, H. Hofmann, and C. Mi, "A double-sided LCLC-compensated capacitive power transfer system for electric vehicle charging," *IEEE Trans. Power Electron.*, vol. 30, no. 11, pp. 6011–6014, Nov. 2015.

[20] J. Dai and D. C. Ludois, "Capacitive power transfer through a conformal bumper for electric vehicle charging," *IEEE J. Emerg. Sel. Topics Power Electron.*, vol. 4, no. 3, pp. 1015–1025, Sep. 2016.

[21] H. Zhang, F. Lu, H. Hofmann, W. Liu, and C. C. Mi, "A four-plate compact capacitive coupler design and LCL-compensated topology for capacitive power transfer in electric vehicle charging application," *IEEE Trans. Power Electron.*, vol. 31, no. 12, pp. 8541–8551, Dec. 2016.

[22] J. Dai, S. S. Hagen, and D. C. Ludois, "Linear motion system cable elimination via multiphase capacitive power transfer through sliding journal bearings," in *Proc. IEEE Appl. Power Electron. Conf. Expo. (APEC)*, Mar. 2017, pp. 2157–2164.

[23] H. Zhang, F. Lu, H. Hofmann, W. Liu, and C. C. Mi, "An LC-compensated electric field repeater for long-distance capacitive power transfer," *IEEE Trans. Ind. Appl.*, vol. 53, no. 5, pp. 4914–4922, Sep. 2017.

[24] H. Zhang, F. Lu, H. Hofmann, W. Liu, and C. C. Mi, "Six-plate capacitive coupler to reduce electric field emission in large air-gap capacitive power transfer," *IEEE Trans. Power Electron.*, vol. 33, no. 1, pp. 665–675, Jan. 2018.

[25] F. Lu, H. Zhang, H. Hofmann, and C. C. Mi, "A double-sided LC-compensation circuit for loosely coupled capacitive power transfer," *IEEE Trans. Power Electron.*, vol. 33, no. 2, pp. 1633–1643, Feb. 2018.

[26] H. Zhang and F. Lu, "An improved design methodology of the double-sided LC-compensated CPT system considering the inductance detuning," *IEEE Trans. Power Electron.*, vol. 34, no. 11, pp. 11396–11406, Nov. 2019.

[27] S. Sinha, A. Kumar, B. Regensburger, and K. K. Afridi, "A new design approach to mitigating the effect of parasitics in capacitive wireless power transfer systems for electric vehicle charging," *IEEE Trans. Transport. Electrific.*, vol. 5, no. 4, pp. 1040–1059, Dec. 2019.

[28] B. Regensburger, S. Sinha, A. Kumar, S. Maji, and K. K. Afridi, "High-performance multi-MHz capacitive wireless power transfer system for EV charging utilizing interleaved-foil coupled inductors," *IEEE J. Emerg. Sel. Topics Power Electron.*, vol. 10, no. 1, pp. 35–51, Feb. 2022.

[29] C. D. Rouse, S. R. Cove, Y. Salami, P. Arsenault, and A. Bartlett, "Three-phase resonant capacitive power transfer for rotary applications," *IEEE J. Emerg. Sel. Topics Power Electron.*, vol. 10, no. 1, pp. 160–169, Feb. 2022.

[30] Y. Liu, T. Wu, and M. Fu, "Interleaved capacitive coupler for wireless power transfer," *IEEE Trans. Power Electron.*, vol. 36, no. 12, pp. 13526–13535, Dec. 2021.

[31] V. Vu, M. Dahidah, V. Pickert, and V. Phan, "An improved LCL-L compensation topology for capacitive power transfer in electric vehicle charging," *IEEE Access*, vol. 8, pp. 27757–27768, 2020.

[32] W. Zhou, Q. Gao, R. Mai, Z. He, and A. P. Hu, "Design and analysis of a CPT system with extendable pairs of electric field couplers," *IEEE Trans. Power Electron.*, vol. 37, no. 6, pp. 7443–7455, Jun. 2022.

[33] W. Liu, B. Luo, Y. Xu, S. Pan, W. Zhou, C. Jiang, and R. Mai, "A multi-load capacitive power transfer system with load-independent characteristic for reefer container application," *IEEE Trans. Power Electron.*, vol. 37, no. 5, pp. 6194–6205, May 2022.

[34] Y. Wang, H. Zhang, and F. Lu, "3.5-kW 94.2% DC–DC efficiency capacitive power transfer with zero reactive power circulating," *IEEE Trans. Power Electron.*, vol. 38, no. 2, pp. 1479–1484, Feb. 2023.

[35] X. Wei, X. Shen, J. Song, Z. Yao, Z. Cao, Y. Zhu, J. Jiang, and H. Ma, "A circuit design method for constant voltage output with zero phase angle and minimum coupler voltages in capacitive power transfer," *IEEE Trans. Power Electron.*, vol. 38, no. 3, pp. 4181–4192, Mar. 2023.

[36] H. Mahdi, B. Hoff, P. G. Ellingsen, and T. Østrem, "Conformal transformation analysis of capacitive wireless charging," *IEEE Access*, vol. 10, pp. 105621–105630, 2022.

[37] C. Liu, A. P. Hu, and M. Budhia, "A generalized coupling model for capacitive power transfer systems," in *Proc. 36th Annu. Conf. IEEE Ind. Electron. Soc.*, Nov. 2010, pp. 274–279.

[38] C. Liu, A. P. Hu, B. Wang, and N. C. Nair, "A capacitively coupled contactless matrix charging platform with soft switched transformer control," *IEEE Trans. Ind. Electron.*, vol. 60, no. 1, pp. 249–260, Jan. 2013.

[39] N. Sakai, D. Itokazu, Y. Suzuki, S. Sakihara, and T. Ohira, "One-kilowatt capacitive power transfer via wheels of a compact electric vehicle," in *Proc. IEEE Wireless Power Transf. Conf. (WPTC)*, May 2016, pp. 1–3.

[40] K. Yi, "Capacitive coupling wireless power transfer with quasi-LLC resonant converter using electric vehicles' windows," *Electronics*, vol. 9, no. 4, p. 676, Apr. 2020.

[41] J. Lian and X. Qu, "Design of a double-sided LC compensated capacitive power transfer system with capacitor voltage stress optimization," *IEEE Trans. Circuits Syst. II, Exp. Briefs*, vol. 67, no. 4, pp. 715–719, Apr. 2020.

[42] D. C. Ludois, M. J. Erickson, and J. K. Reed, "Aerodynamic fluid bearings for translational and rotating capacitors in noncontact capacitive power transfer systems," *IEEE Trans. Ind. Appl.*, vol. 50, no. 2, pp. 1025–1033, Mar. 2014.

[43] T. M. Mostafa, A. Muharam, A. Patrick Hu, and R. Hattori, "Improved CPT system with less voltage stress and sensitivity using a step-down transformer on receiving side," *IET Power Electron.*, vol. 12, no. 10, pp. 2634–2641, Aug. 2019.

[44] S. Zang and S. K. Nguang, "Capactive power transfer design for multiple receivers on conveyors," in *Proc. 45th Annu. Conf. IEEE Ind. Electron. Soc.*, vol. 1, Oct. 2019, pp. 4183–4188.

[45] J. Dai, S. S. Hagen, and D. C. Ludois, "High-efficiency multiphase capacitive power transfer in sliding carriages with closed-loop burst-mode current control," *IEEE J. Emerg. Sel. Topics Power Electron.*, vol. 7, no. 2, pp. 1388–1398, Jun. 2019.

[46] S. Ahmad, A. Muharam, R. Hattori, A. Uezu, and T. M. Mostafa, "Shielded capacitive power transfer (S-CPT) without secondary side inductors," *Energies*, vol. 14, no. 15, p. 4590, Jul. 2021.

[47] A. Muharam, S. Ahmad, R. Hattori, and A. Hapid, "13.56 MHz scalable shielded-capacitive power transfer for electric vehicle wireless charging," in *Proc. IEEE PELS Workshop Emerg. Technol., Wireless Power Transf. (WoW)*, Nov. 2020, pp. 298–303.

[48] S. Li, Z. Liu, H. Zhao, L. Zhu, C. Shuai, and Z. Chen, "Wireless power transfer by electric field resonance and its application in dynamic charging," *IEEE Trans. Ind. Electron.*, vol. 63, no. 10, pp. 6602–6612, Oct. 2016.

[49] *Electromagnetic Compatibility (EMC)—Part 6–1: Generic Standards—Immunity Standard for Residential, Commercial and Light-Industrial Environments*, International Electrotechnical Commission, London, U.K., 2016.

[50] Z. Chen, P. Davari, and H. Wang, "Single-phase bridgeless PFC topology derivation and performance benchmarking," *IEEE Trans. Power Electron.*, vol. 35, no. 9, pp. 9238–9250, Sep. 2020.

[51] Z. Chen, B. Liu, Y. Yang, P. Davari, and H. Wang, "Bridgeless PFC topology simplification and design for performance benchmarking," *IEEE Trans. Power Electron.*, vol. 36, no. 5, pp. 5398–5414, May 2021.

[52] F. Lu, H. Zhang, and C. Mi, "A two-plate capacitive wireless power transfer system for electric vehicle charging applications," *IEEE Trans. Power Electron.*, vol. 33, no. 2, pp. 964–969, Feb. 2018.

[53] S. Ahmad, R. Hattori, and A. Muharam, "Generalized circuit model of shielded capacitive power transfer," *Energies*, vol. 14, no. 10, p. 2826, May 2021.
[54] C. G. Montgomery, R. H. Dicke, and E. M. Purcell, *Principles of Microwave Circuits (Electromagnetic Waves)*. Edison, NJ, USA: IET, 1987.
[55] D. M. Pozar, *Microwave Engineering*, 4th ed. Hoboken, NJ, USA: Wiley, 2011.
[56] L. Pamungkas, S. Wu, and H. Chiu, "Equivalent circuit approach for output characteristic design of capacitive power transfer," *IEEE Trans. Circuits Syst. II, Exp. Briefs*, vol. 68, no. 7, pp. 2513–2517, Jul. 2021.
[57] H. Mahdi, B. Hoff, and T. Østrem, "Optimal solutions for underwater capacitive power transfer," *Sensors*, vol. 21, no. 24, p. 8233, Dec. 2021.
[58] T. Ohira, "Extended k-Q product formulas for capacitive- and inductive-coupling wireless power transfer schemes," *IEICE Trans. Electron.*, vol. 11, no. 9, pp. 1–7, 2014.
[59] M. Tamura, Y. Naka, and K. Murai, "Design of capacitive coupler in underwater wireless power transfer focusing on kQ product," *IEICE Trans. Electron.*, vol. 10, pp. 759–766, Jan. 2018.
[60] S. Friedel. (Oct. 2, 2023). *How to Calculate a Capacitance Matrix in Comsol Multiphysics*. [Online]. Available: https://www.comsol.com/blogs/how-to-calculate-a-capacitance-matrix-in-comsol-multiphysics/
[61] E. Bracken and G. Pitner. (Feb. 10, 2023). *Module 4: Q3D Capacitance Matrix Reduction*. [Online]. Available: https://courses.ansys.com/wp-content/uploads/2021/07
[62] Comsol. (Feb. 10, 2023). *Computing the Effect of Fringing Fields on Capacitance*. [Online]. Available: https://www.comsol.jp/model/computing-the-effect-of-fringing-fields-on-capacitance-12605
[63] *Advanced Impedance Measurement Capability of the RF I–V Method Compared to the Network Analysis Method—Application Note 1369-2*, Agilent Technologies, Santa Clara, CA, USA, 2001.
[64] M. Horibe, "Performance comparisons between impedance analyzers and vector network analyzers for impedance measurement below 100 MHz frequency," in *Proc. 89th ARFTG Microw. Meas. Conf. (ARFTG)*, Jun. 2017, pp. 1–4.
[65] H. Zhang, F. Lu, H. Hofmann, and C. Mi, "A loosely coupled capacitive power transfer system with LC compensation circuit topology," in *Proc. IEEE Energy Convers. Congr. Expo. (ECCE)*, Sep. 2016, pp. 1–5.
[66] S. Sinha, A. Kumar, B. Regensburger, and K. K. Afridi, "Design of high-efficiency matching networks for capacitive wireless power transfer systems," *IEEE J. Emerg. Sel. Topics Power Electron.*, vol. 10, no. 1, pp. 104–127, Feb. 2022.
[67] A. Amler, N. Weitz, and M. März, "Improved capacitive power transfer with non-resonant power transfer link using radio frequency push-pull inverter," *IEEE J. Emerg. Sel. Topics Power Electron.*, vol. 10, no. 6, pp. 7808–7823, Dec. 2022.
[68] K. Akiyoshi, R. Hattori, and A.-Y. Uezu, "High frequency shielded-capacitive power transfer system with resonance rectifier," in *Proc. Asian Wireless Power Transf. Workshop*, 2022, pp. 1–4.
[69] *Guidelines for Limiting Exposure to Electromagnetic Fields (100 kHz to 300 GHz)*, ICNIRP, Munich, Germany, 2020.
[70] A. Muharam, S. Ahmad, and R. Hattori, "Scaling-factor and design guidelines for shielded-capacitive power transfer," *Energies*, vol. 13, no. 16, p. 4240, Aug. 2020.
[71] B. Luo, R. Mai, Y. Chen, Y. Zhang, and Z. He, "A voltage stress optimization method of capacitive power transfer charging system," in *Proc. IEEE Appl. Power Electron. Conf. Expo. (APEC)*, Mar. 2017, pp. 1456–1461.
[72] R. Mai, B. Luo, Y. Chen, and Z. He, "Double-sided CL compensation topology based component voltage stress optimisation method for capacitive power transfer charging system," *IET Power Electron.*, vol. 11, no. 7, pp. 1153–1160, Jun. 2018.
[73] S. Yang, Y. Zhang, Y. Zhang, Y. Wang, Z. Wang, B. Luo, and R. Mai, "Analysis and design of a dual-frequency capacitive power transfer system to reduce coupler voltage stress," *Electronics*, vol. 12, no. 6, p. 1274, Mar. 2023.
[74] A. Muharam, S. Ahmad, R. Hattori, D. Obara, M. Masuda, K. Ismail, and A. Hapid, "An improved ground stability in shielded capacitive wireless power transfer," in *Proc. Int. Conf. Sustain. Energy Eng. Appl. (ICSEEA)*, Oct. 2019, pp. 1–5.
[75] B. Regensburger, A. Kumar, S. Sinha, and K. K. Afridi, "Impact of foreign objects on the performance of capacitive wireless charging systems for electric vehicles," in *Proc. IEEE Transp. Electrific. Conf. Expo (ITEC)*, Jun. 2018, pp. 892–897.

HUSSEIN MAHDI (Graduate Student Member, IEEE) received the M.Sc. degree in electrical engineering from UiT The Arctic University of Norway, in 2019, where he is currently pursuing the Ph.D. degree. He is also a Graduate Researcher with UiT The Arctic University of Norway. His research interests include resonant converters, soft switching, wireless power transfer, and power factor correction.

REIJI HATTORI (Member, IEEE) received the B.S. and M.S. degrees in electrical engineering and the Ph.D. degree from Osaka University, Japan, in 1986, 1988, and 1992, respectively. He became a Research Associate with the Department of Electrical Engineering, Osaka University, in 1989. In 1997, he moved to Kyushu University, Fukuoka, Japan, as an Associate Professor, where he was promoted to Professor, in 2009. He is currently working on display and related technologies, including OLED, touch panels, and wireless power transfer systems. He is a member of SID, IEICE, and JSAP.

BJARTE HOFF (Senior Member, IEEE) received the B.S. degree in maritime electro automation from Vestfold University College, Borre, Norway, in 2008, the M.Sc. degree in electrical engineering from Narvik University College, Narvik, Norway, in 2010, and the Ph.D. degree in electrical power engineering from the Norwegian University of Science and Technology (NTNU), in 2016.

He was certified as an Electrician, in 2004. His research interests include power electronics with application within future energy system and electric transport, two inspiring areas that are important for the transition to a sustainable future. The use of power conversion technology through power electronics and associated control algorithms is essential for renewable energy, electric transport and energy storage. Charging of electric vehicles, maritime vessels and aircrafts is combining all those research areas on both component and system level, representing an important element for the electric future.

ANYU UEZU received the M.Sc. degree in engineering from the Interdisciplinary Graduate School of Engineering Sciences, Kyushu University, Japan, in 2023. His research interests include wireless power transfer and electric vehicles.

KATSUMI AKIYOSHI received the B.Sc. degree in engineering from Ryukyu University, Japan, in 2022. He is currently pursuing the M.Sc. degree in engineering with the Interdisciplinary Graduate School of Engineering Sciences, Kyushu University, Japan. His research interests include wireless power transfer, electric vehicles, and robot arms. He is a member of IEICE and SID.